

A Possible Correlation between Metallicity and Near-IR Color for Late-M and L Dwarfs

RUIHAN ZHANG (张瑞涵) ¹, MICHAEL C. LIU ², AND ZHOUIAN ZHANG (张周健) ^{3,*}

¹*Institute for Astronomy, University of Hawai'i
Hilo, HI 96720, USA*

²*Institute for Astronomy, University of Hawai'i
Honolulu, HI 96822, USA*

³*Department of Astronomy & Astrophysics, University of California, Santa Cruz, CA 95064, USA*

ABSTRACT

We examine the relationship between metallicity and $J - K$ color for 64 benchmark late-M and L dwarfs, all of which are wide companions to higher mass stars, and 6 of which are new discoveries. We assess the correlation between the $\Delta(J - K)$ color anomaly (the difference of an object's $J - K$ color with the median color for field objects of the same spectral type) and the host star metallicity to investigate how metallicity affects ultracool photospheres. Using Spearman's rank correlation test and Student's t test, the late-M dwarf (L dwarf) sample's $\Delta(J - K)$ and metallicity show a positive correlation with 95% (90%) confidence level. A linear fit to color anomaly as a function of metallicity finds a slope of 0.17 ± 0.07 for the late-M dwarfs and a slope of $0.20^{+0.07}_{-0.08}$ for the L dwarfs. We also computed the $\Delta(J - K)$ versus metallicity relationship predicted by multi-metallicity model spectra generated using Drift-Phoenix. The modeled late-M dwarfs show a slope of 0.202 ± 0.03 , which is close to our observational results, but the modeled L dwarfs show a slope of 0.493 ± 0.02 , steeper than our observational results. Both our empirical results and the models indicate that more metal-rich objects should appear redder photometrically. We speculate that higher metallicity drives more condensate formation in these atmospheres, thus making these ultracool dwarfs appear redder.

Keywords: Brown dwarfs(185) — L dwarfs(894) — Metallicity(1031) — Photometry(1234)

1. INTRODUCTION

Understanding the atmospheres of ultracool dwarfs (late-M, L, and T dwarfs) is particularly interesting because they span similar temperature and mass regimes as giant exoplanets. Thus learning more about ultracool dwarfs would help us better understand the atmospheres of the giant planets outside of our solar system. In contrast to higher mass stars, which follow a narrow sequence on the color-magnitude diagrams (CMD) in the near-IR (NIR), the photometry of ultracool dwarfs show a significant spread. Some of the spread can be attributed to variations in surface gravity (Knapp et al. 2004, Liu et al. 2016), which is related to the mass and age spread of these objects. Low gravity objects, or young objects, appear redder in NIR photometry compared to the field objects of the same spectral types. The viewing geometry of the ultracool dwarfs also plays a role in creating color anomalies in ultracool dwarf photometry (Vos et al. 2017, Toro et al. 2022). When ultracool dwarfs are viewed at larger inclination angles, they would appear redder in the NIR colors. Other factors may also be contributors to the observed diversity of ultracool dwarfs' NIR photometry. Metallicity, one of the fundamental parameters that contribute to the physical properties of stars, is expected to also affect the photometry of ultracool dwarfs (Burrows et al. 2001, Saumon & Marley 2008, Fortney et al. 2008, Marley et al. 2021). In this work, we aim to collect a sample of ultracool dwarfs with metallicity information to investigate the relationship between the metallicity and photometric properties of these objects.

Corresponding author: Ruihan Zhang
rzhang9@hawaii.edu

* NASA Sagan Fellow

Late-M (M6-M9) and L dwarfs are known to have cloudy atmospheres with silicate condensates that are optically thick in the NIR (e.g., Burrows & Sharp 1999, Marley & Ackerman 2001, Lodders 2002, Allard et al. 2011). These silicates then dissipate and settle deeper into the atmosphere as brown dwarfs cool into early-T dwarfs and later spectral types (e.g., Marley et al. 2002, Lodders & Fegley 2006, Zhang et al. 2021a). Other species of clouds such as water, chlorides, and sulfides start to form in the cooler atmospheres of T dwarfs and later spectral types, but they are physically and optically thin in the NIR, making them effectively "cloudless" (Visscher et al. 2006, Morley et al. 2012, Morley et al. 2014, Lacy & Burrows 2023). Therefore, mid/late-T dwarfs' NIR photometry is not affected by clouds the same way as the late-M and L dwarfs. Detailed studies of condensate formation and other related processes in ultracool dwarfs' atmospheres are still in progress (e.g., Allard 2014, Marley & Robinson 2015). One possible cause for the variation in late-M and L dwarfs' NIR colors is that the amount of cloud formation is correlated with metallicity of the ultracool dwarfs.

By establishing a sample of late-M and L dwarfs with known metallicities, we can investigate the imprints of atmospheric composition on the photometry of these objects. However, there is a paucity of detailed studies on metallicity properties for late-M and L dwarfs. The reason for this is measuring the metallicity of these cool objects is difficult due to their molecule-rich atmospheres. The many molecular lines/bands in their spectra hinder accurate extraction of ultracool dwarfs' metallicity information. Many strong efforts have been put into accurately measuring the metallicity of these objects by fitting low-temperature atmospheric models, such as Line et al. (2015), Zalesky et al. (2019), Zhang et al. (2021b), Xuan et al. (2022), and Hood et al. (2023), etc. These measurements are subject to modeling systematics. Another common way to study the metallicity properties of the ultracool dwarfs is when they are companions of brighter stars (e.g. Mann et al. 2014). By measuring the metallicity of the host stars and assuming the primary and the secondary objects formed from the same molecular cloud, we can infer the metallicities of the ultracool companions from the metallicities of their host stars. This method provides us higher accuracy metallicity measurements of ultracool dwarf companions. We refer to these companions as 'benchmark objects' given that some of their physical properties are known from independent information.

In this work we focus on studying how metallicity is correlated with late-M and L dwarfs' observed near-IR colors, seeking to insight into whether metallicity affects the condensate formation in their atmospheres. We gathered a sample of late-M and L dwarf benchmarks (Section 2), performed a correlation analysis for their ($J - K$) color and metallicity (Section 3), and compared these results with multi-metallicity atmospheric models (Section 4). In addition, we discuss the possibility of using the empirical relationships we find as an easy and efficient method to provide bulk metallicity estimates for late-M and L dwarfs given their NIR photometry (Section 5).

2. SAMPLE SELECTION

To study the correlation between metallicity and near-IR photometry for late-M and L dwarfs, we constructed a sample of benchmark late-M and L companions that have both $J - K$ colors and metallicity measurements of their host stars. $J - K$ was chosen because most M and L dwarfs have J and K photometry, making it a color commonly used in the study of ultracool dwarfs. As described below, we gathered late-M and L dwarf companions from the *UltracoolSheet* (Best et al. 2020) and Mann et al. (2014). Additionally, we identified 6 new benchmark ultracool dwarfs using the El-Badry et al. (2021) binary catalog. Our total sample consisted of 67 objects, including 35 late-M dwarfs and 32 L dwarfs.

2.1. Previously Known Benchmarks

The *UltracoolSheet* (UCS) is a library of 3000+ ultracool dwarfs with spectral types, photometry, astrometry, multiplicity, and companion information. The UCS provides both optical and IR spectral types when available. Following the field convention, the optical spectral types were used whenever available. Otherwise, the IR spectral types were used. For most objects in our selected sample with both optical and IR spectral types, their optical and IR spectral types are the same. There are only two objects with the largest discrepancy of half a spectral type between optical and IR. As for metallicity, we obtained the benchmark objects' metallicities by finding their primary stars in APOGEE (Majewski et al. 2017) and Hypatia (Hinkel et al. 2014). ASPCAP (García Pérez et al. 2016), the spectral fitting pipeline for measuring chemical abundances in APOGEE, uses solar normalization from Asplund et al. (2005) for its metallicity measurements. To ensure consistency, we queried Hypatia metallicities with the same solar normalization. For objects that were not in APOGEE nor Hypatia, we checked SIMBAD for metallicity information from literature. In total, we gathered 17 late-M dwarf companions and 30 L dwarf companions with known metallicities

from the UCS. Young objects and subdwarfs were excluded from the sample because they have different photometric properties compared to the field objects.

Mann et al. (2014) contains a list of mid- to late-M dwarfs with known metallicities that they used to study metallicity calibrations for ultracool dwarfs. The metallicity measurements were carefully fitted and calibrated by using high resolution spectra and Spectroscopy Made Easy (SME; Valenti & Piskunov 1996). We included the late-M dwarfs in this study as part of our sample, which added an additional 11 late-M dwarfs with known metallicities to our total sample. Mann et al. (2014) provided the IR spectral types of these objects.

2.2. Mining the El-Badry et al. (2021) binary catalog

To increase our benchmark sample, we mined the El-Badry et al. (2021) binary catalog for late-M dwarfs and L dwarfs. The El-Badry et al. (2021) catalog contains 1.3 million spatially resolved binaries within ~ 1 kpc of the Sun identified from Gaia eDR3 (Gaia Collaboration et al. 2021). We used *Phototype*, a spectral energy distribution (SED) fitting method introduced by Skrzypek et al. (2015), to identify late-M dwarfs and L dwarfs using photometry from large sky surveys. *Phototype* summarizes a library of known objects as polynomial fits to colors as a function of spectral type (SpT). In our case, the UCS and Best et al. (2018a) was used to build the color functions with *grizy* band data from Pan-STARRS 1 (PS1; Chambers et al. 2016), *JHK* band data from the Mauna Kea observatories (MKO; Dye et al. 2018, Dahm et al. 2018, Lawrence et al. 2007), and *W1* and *W2* from CatWISE (Marocco et al. 2021). We used the *W1* band as the reference filter to calculate the colors (e.g., $i - W1$, $W1 - W2$) of each UCS object (excluding binaries, subdwarfs and young objects), because it is available for 85% of objects in our candidate list. The colors were fitted as polynomial functions for spectral types from M0 through Y0 (which corresponds to integers 0 through 30) and were weighted by the inverse square of the photometric errors (Table 1). For each color, only 5th order polynomials were fitted initially, we then successively increased the order as long as a polynomial with $n+1$ orders would bring a significantly improved fit (i.e., $\Delta\chi^2 > 7$) than the n th order polynomial. Then model templates were generated from the polynomial fits for each spectral type and least-squares fitting was performed on each secondary star in the El-Badry et al. (2021) catalog with suitable photometry. A secondary star is then assigned the spectral type of the model template that results in the lowest χ^2 .

Before spectral typing the secondary objects in the El-Badry et al. (2021) binary catalog with the SED fitting algorithm, we first placed a distance limit of 200 pc on the catalog. The 200 pc limit was chosen because most L dwarfs should have at least 6 bands of photometry out to this distance, that could enable a robust spectral typing for *Phototype*. Then we retrieved photometry of the companions from PS1 (Chambers et al. 2016), the Two Micron All Sky Survey (2MASS; Skrutskie et al. 2006), the UKIRT Hemisphere Survey (UHS; Dye et al. 2018), the *UKIRT Infrared Deep Sky Survey* (UKIDSS; Lawrence et al. 2007), and CatWISE (Marocco et al. 2021). For objects that have *JHK* band data in the MKO photometric system, including UHS and UKIDSS, their MKO measurements are used instead of 2MASS. For objects with only 2MASS data, we convert their photometry to the MKO system using formulas from Stephens & Leggett (2004), because our SED templates use the MKO system. We further limit the sample to objects that have at least 4 bands of photometry.

Using the best-fit SpT from *Phototype*, we compared our candidates' SpTs and absolute G-band magnitudes from Gaia (Gaia Collaboration et al. 2021) to the G-band absolute magnitude versus SpT trend calculated from ultracool dwarfs in the UCS. Candidates with fitted SpT ranging from M9 to L9 that fell within ± 2 mag of the known G-band trend were studied by looking at their PS1 image cutouts to confirm that the objects are point sources. Then, we examined the χ^2 as a function of template SpT resulting from the SED fits, selecting objects with well-defined χ^2 minima. We identified 14 ultracool dwarfs among these secondary stars, of which 6 are new discoveries (4 late-M dwarfs and 2 L dwarfs). Their SEDs correspond well to the best-fit SED templates (Figure 1). The 6 discoveries also land on the correct place on the color magnitude diagram (Figure 2), further indicating that they have accurate spectral type estimates. Then, similar to the objects we gathered from the UCS, we crossmatched the host stars of these 6 objects to the APOGEE (Majewski et al. 2017) and Hypatia (Hinkel et al. 2014) catalogs to obtain their metallicity information.

Adding these 6 new objects to the sample gathered from the UCS and Mann et al. (2014), we ended up with a final sample of 64 objects: 32 late-M dwarfs (Table 3) and 32 L dwarfs (Table 4).

3. CORRELATION ANALYSIS

As shown in Figure 2, the $J - K$ colors of ultracool dwarfs follow a defined trend. However, different physical processes that take place in the atmospheres of these objects can cause color variations, making some objects appear

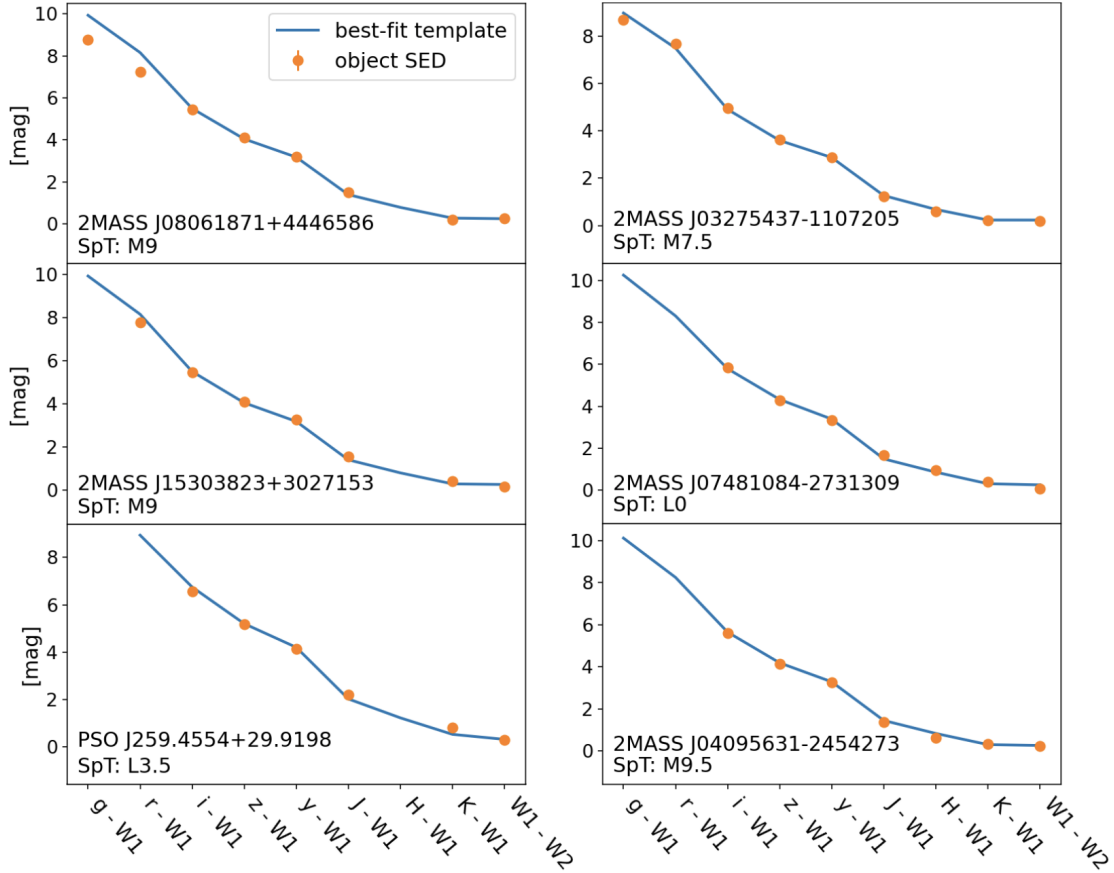


Figure 1. Spectral energy density of the 6 ultracool dwarfs identified from the [El-Badry et al. \(2021\)](#) binary catalog that are not in the UCS. Error bars for the photometry are smaller than the symbol size.

redder or bluer than others. In our case, we want to understand how metallicity affects the photometry of ultracool dwarfs. Therefore, we calculated the $J - K$ color for all our benchmarks and compared them to the median $J - K$ color (Table 2) for each SpT (calculated using all objects in the UCS excluding binaries, subdwarfs, and young objects) using the MKO photometric system (Figure 3). The difference between the $J - K$ color of each object and the median of its SpT, known as $J - K$ anomaly and denoted as $\Delta(J - K)$, was calculated and plotted as a function of $[\text{Fe}/\text{H}]$ (Figure 4).

Within our sample, there are 7 objects (2 late-M dwarfs and 5 L dwarfs) that have published metallicities without reported uncertainties. These objects were omitted in the correlation analysis, but they are still presented in Figure 4 to show that there are no significant outliers in our sample. Hence, our correlation analysis was performed using the remaining 57 objects that have both $J - K$ color and metallicity. In the sample, 11 objects use metallicities from APOGEE, 17 from Hypatia, and 14 from [Mann et al. \(2014\)](#). The remaining 15 objects use metallicity measurements from other various sources documented in Table 3 and 4.

As mentioned in Section 2, APOGEE and Hypatia both use solar normalization from [Asplund et al. \(2005\)](#). [Mann et al. \(2014\)](#) and APOGEE both use spectral fitting for measuring the stellar abundances. Metallicity measurements from the literature are not necessarily calibrated with each other, e.g. different sources most likely do not use the same normalization and methods, whether it be spectral fitting or curve of growth. The inconsistencies may inject extra systematic uncertainties in our analysis. [Hinkel et al. \(2014\)](#) found a median error of 0.04 dex across metallicities calibrated with different solar normalizations, which is a small effect compared to the metallicity range of our sample. Nonetheless, we made an effort to use metallicity measurements from APOGEE and Hypatia whenever possible. Due to these unaccounted uncertainties, the errors in our analysis represent the error floor. We performed the same correlation analysis for three sets of data: the total sample of 57 ultracool dwarfs, the 30 late-M dwarfs, and the 27 L dwarfs.

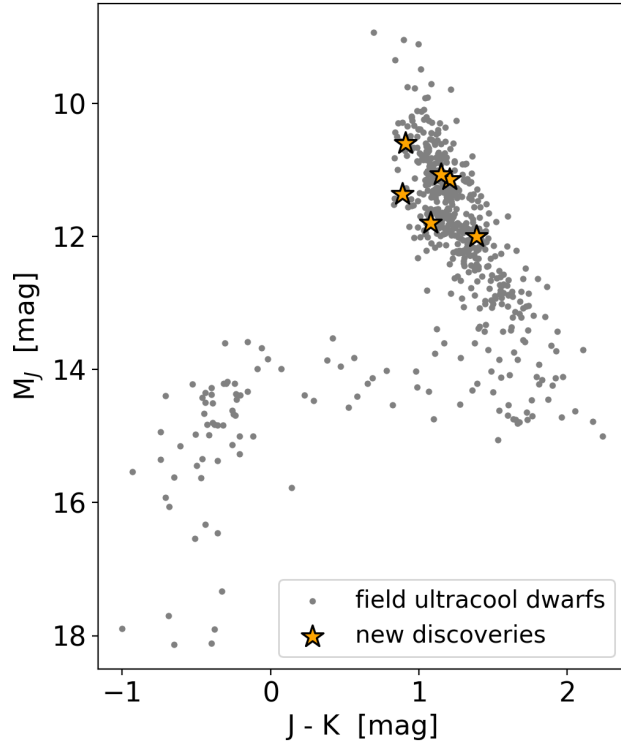


Figure 2. Color magnitude diagram of our 6 discovered ultracool companions (yellow stars) compared to field dwarfs in the UCS (grey dots).

We used Spearman’s rank correlation coefficient to examine whether the color anomaly $\Delta(J - K)$ and $[\text{Fe}/\text{H}]$ are correlated. To account for measurement uncertainties, we simulated random samples of the data assuming Gaussian errors and ran 10,000 iterations of the test. A small fraction of the sample have implausibly small photometric errors (≤ 0.01 mag) reported from UKIDSS, which were computed by direct error propagation of the flux error using the formula $\sigma_{mag} = \frac{2.5}{\ln(10)} \frac{\sigma_f}{f}$. We set a floor to these photometric errors of 0.01 mag, which was motivated by fundamental calibration of UKIDSS to 2MASS, so objects with extremely small uncertainties do not skew our analysis. The total sample returned a Spearman’s rank correlation coefficient (and standard deviation) of 0.26 ± 0.07 and its corresponding Student’s t value resulted in a $97.5\%_{-7.5\%}^{+1.5\%}$ confidence to reject the null hypothesis, namely that the parameters are not correlated with each other. The late-M dwarfs sample had a correlation coefficient of 0.31 ± 0.10 corresponding to a $95\%_{-10\%}^{+2\%}$ confidence level. And the L dwarfs sample resulted in a Spearman’s rank correlation coefficient of 0.32 ± 0.11 and a $90\%_{-5\%}^{+8\%}$ confidence level. This suggests that both late-M and L dwarfs show correlation between $\Delta(J - K)$ and $[\text{Fe}/\text{H}]$ with high confidence level.

In attempt to summarize our observation and formulate an empirical relationship between $J - K$ anomaly and metallicity for late-M and L dwarfs, we applied 2 linear regression methods to fit the data. First, we drew random samples of the data assuming Gaussian errors for both $\Delta(J - K)$ and $[\text{Fe}/\text{H}]$, then we used Ordinary Least Squares (OLS) to fit the drawn samples to linear models. This Monte Carlo (MC) process was repeated 1,000,000 iterations for the late-M dwarfs and the L dwarfs separately. The late-M dwarfs were best-fit to a slope of 0.17 ± 0.07 and a constant of -0.08 ± 0.01 ; the L dwarfs resulted in a fitted slope of $0.20_{-0.08}^{+0.07}$ with a constant of -0.01 ± 0.02 for the L-dwarfs ($J - K$) anomaly and metallicity (Figure 4). This means for both populations, the more metal rich the objects appear to have redder $J - K$ colors. We speculate that the presence of more metals induces more condensate formation in the atmospheres of late-M and L dwarfs, thus making them appear redder in the NIR compared to objects of similar SpT but lower metallicity. In the following section, we show a comparison of our empirical findings with synthetic L

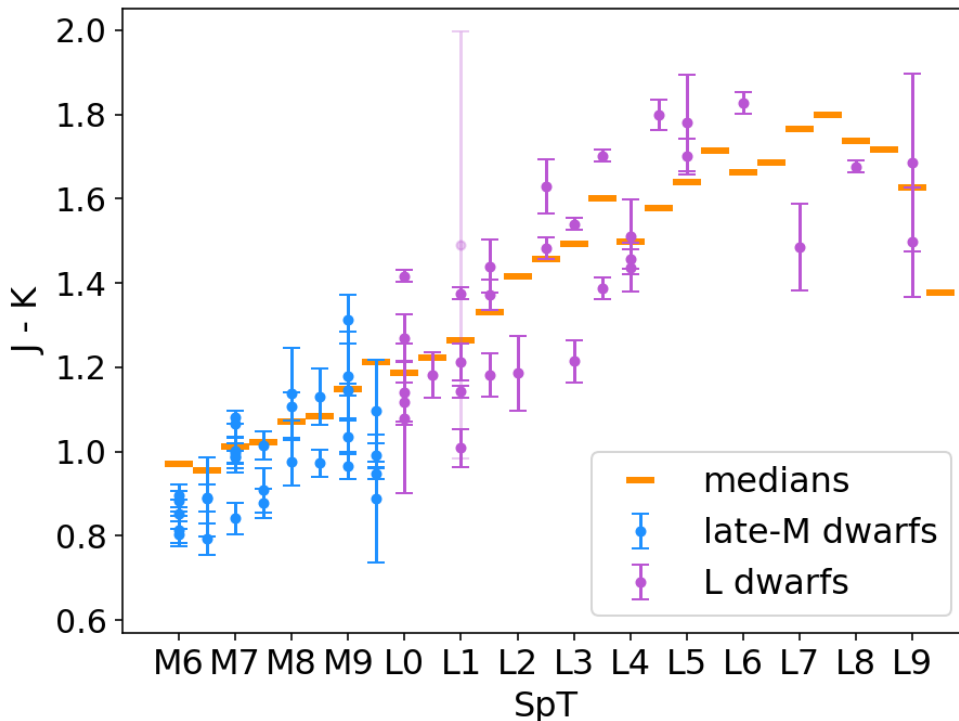


Figure 3. $J - K$ color of our late-M and L sample compared with the median $J - K$ colors of each SpT. Objects with signal to noise ratio (SNR) < 3 are plotted in a lighter shade.

dwarf spectra generated from Drift-Phoenix (Dehn et al. 2007; Helling et al. 2008a; Witte et al. 2009) and discuss its significance.

We also experimented with using Orthogonal Distance Regression (ODR; Boggs et al. 1988) for fitting our data to linear models. Using ODR, the late-M dwarfs resulted in a slope of 0.52 ± 0.16 with a constant of -0.07 ± 0.03 ; the L dwarfs were best fit to a slope of 0.48 ± 0.19 and a constant of 0.02 ± 0.04 . Similar to the MC results, $\Delta(J - K)$ has a positive relationship with $[\text{Fe}/\text{H}]$ for both late-M and L dwarfs, but the ODR fits have steeper slopes.

One other detail to note here is that our late-M sample of benchmarks seems to have bluer $J - K$ anomaly than our L sample based on our MC fits. To better understand the populations that we are working with and test if the late-M sample is inherently bluer than the L sample, we used the 2-sample Kolmogorov-Smirnov (KS) test to study them. The 2-sample KS test is a standard statistical procedure to test whether two underlying one-dimensional probability distributions differ. The 2-sample KS test showed that we cannot confidently differentiate the late-M and L samples given their $\Delta(J - K)$ distribution (Figure 5) even though they seem bluer in Figure 4. We also performed the 2-sample KS test between our samples with field FGK stars from Casagrande et al. (2011) to assure that their metallicity distributions are consistent with the field stars (Figure 6). The KS tests showed that both the late-M and L samples have metallicity distributions consistent with the field FGK stars.

4. COMPARISON WITH MODEL ATMOSPHERES

It is always valuable to compare observational data to simulated models because observations verify the assumptions that are used for building models. In the iterative process of taking observations, then making assumptions and building models that match the observations, we build more accurate models that better represent the real world. This is common practice to study phenomena that we cannot take direct measurements of. Here, we compare our observed results to the Drift-Phoenix model atmospheres. Drift-Phoenix is a model atmosphere code derived from the PHOENIX code family (Hauschildt & Baron 1999, Baron et al. 2003) and the DRIFT models (Woitke & Helling 2003, 2004; Helling & Woitke 2006; Helling et al. 2008b) that simulate stellar/planetary atmospheres including the formation

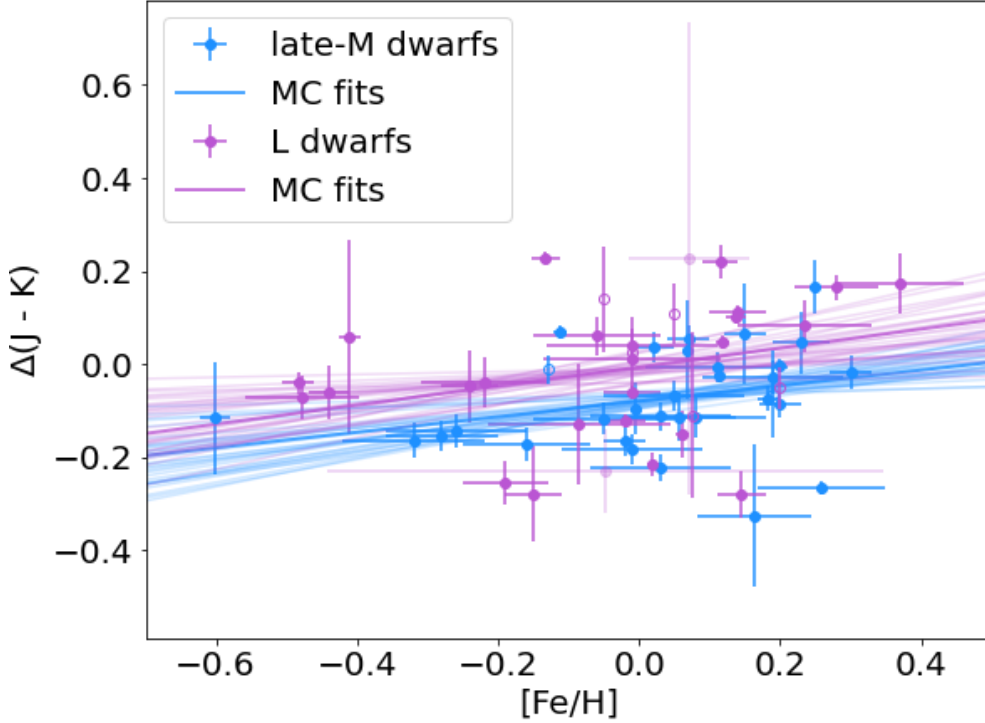


Figure 4. $\Delta(J - K)$ of all objects in the late-M/L sample as a function of $[\text{Fe}/\text{H}]$. Similar to Figure 3, objects with $\text{SNR} < 3$ are plotted in lighter shades. Objects plotted with hollow markers do not have metallicity errors. The lines show 30 samples of the MC fits.

of condensates. Additionally, this set of models is multi-metallicity while most other models that take cloud formation into consideration are not. Hence the Drift-Phoenix models are relevant to this work. Note that the model atmospheres do not fit actual spectra of these objects well, we are only using them in a differential case for color calculations. To study how our observed trend compares with theoretical atmospheric models, we calculated the $J - K$ color of the models: with T_{eff} ranging from 2300 K to 2900 K for the late-M dwarfs (Figure 7) and T_{eff} ranging from 1300 K to 2200 K for the L dwarfs (Figure 9); $\log(g)$ of 4.5, 5.0, and 5.5 $\log(\frac{\text{cm}}{\text{s}^2})$; and metallicities ranged from -0.6 to 0.3 with increments of 0.3. The higher temperature range covers late-M dwarfs while the lower temperature range covers L dwarfs, and the gravity range covers field objects while leaving out young objects. Considering that the late-L dwarfs entering the transient phase of the L-T transition that is not accurately modeled, we limit the temperature range to ≥ 1700 K for the following analysis, which corresponds to SpT earlier than L6 based on the T_{eff} -SpT relationship in Dupuy & Liu (2017).

Given the observational data shows a value close to zero for $\Delta(J - K)$ at solar metallicity, we subtracted the modeled $J - K$ colors by the solar metallicity models and plotted the results as a function of metallicity in Figure 8 and Figure 10 to compare to Figure 4. For the late-M dwarfs, the models resulted in a slope of 0.20 ± 0.03 and a constant of -0.03 ± 0.01 using OLS linear regression. We can see in Figure 8 that the fit is heavily influenced by the widespread data in $\Delta(J - K)$ of various T_{eff} and $\log(g)$. This wide variation is pulling the y-intercept below zero, which is somewhat evocative of the late-M dwarfs' observational data which has a fitted y-intercept of -0.08 ± 0.01 (MC approach). Looking at the fitted slopes, the models' result overlaps with our observational result of 0.17 ± 0.07 , suggesting that the current Drift-Phoenix models are reasonable representations of late-M dwarfs looking from the perspective of this metallicity distribution. For the L dwarfs, the models also show a positive linear relationship (fitted using OLS) with a slope of 0.49 ± 0.02 and a constant of 0.001 ± 0.008 . The slope is a much larger value compared to our MC observational value of $0.20^{+0.07}_{-0.08}$ but in the same direction.

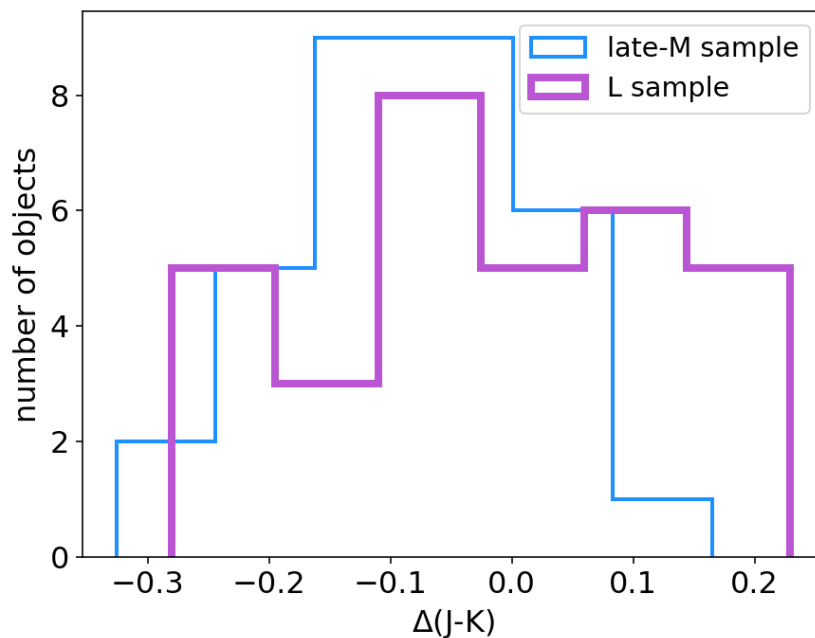


Figure 5. A histogram of our late-M dwarfs and L dwarfs as a function of color anomaly $\Delta(J-K)$.

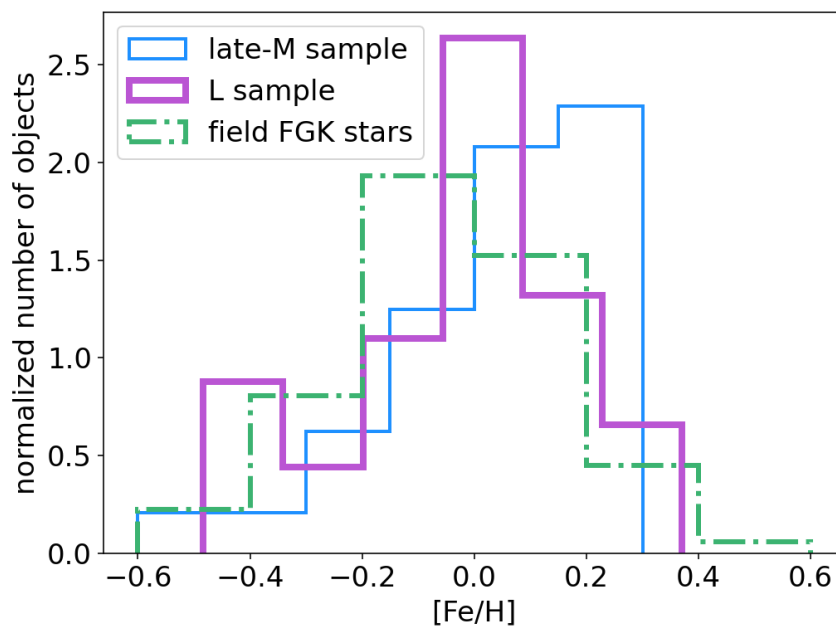


Figure 6. A normalized histogram of our late-M and L dwarfs as a function of metallicity compared to field FGK stars.

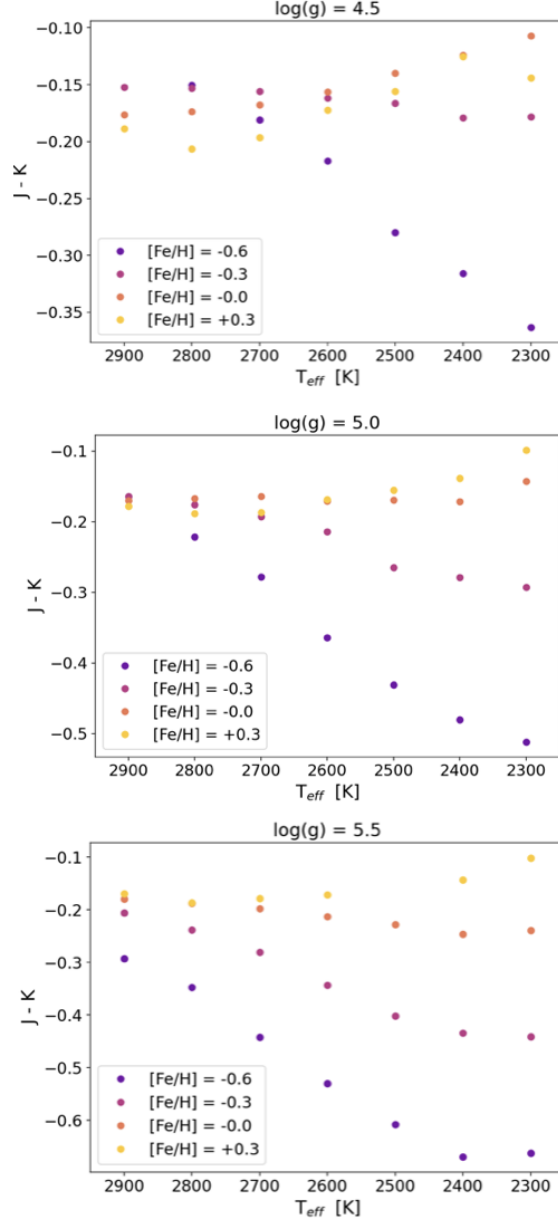


Figure 7. Drift-Phoenix models with a temperature range of [2300 - 2900 K] and a $\log(g)$ range of [4.5, 5.0, 5.5] $\log(\frac{cm}{s^2})$, which corresponds to late-M dwarfs. All photometry is on the MKO system.

5. EMPIRICAL RELATIONSHIPS FOR PHOTOMETRIC METALLICITIES OF LATE-M AND L DWARFS

Past studies have found empirical relationships between $J - K$ color and metallicity of M-dwarfs, which can provide a convenient way for obtaining the metallicity of objects from photometry alone. For example, partly based on the color-metallicity relationship noted in Leggett (1992) and Lépine & Shara (2005), Johnson et al. (2012) found an empirical relationship between metallicity and $J - K$ using a volume-limited M dwarf sample:

$$[Fe/H] = -0.050 + 3.520\Delta(J - K) \quad (1)$$

where $\Delta(J - K)$ is defined as

$$\Delta(J - K) = \begin{cases} (J - K) - 0.835 & (V - K) < 5.5 \\ (J - K) - \sum_{i=0} a_i (V - K)^i & (V - K) \geq 5.5 \end{cases}$$

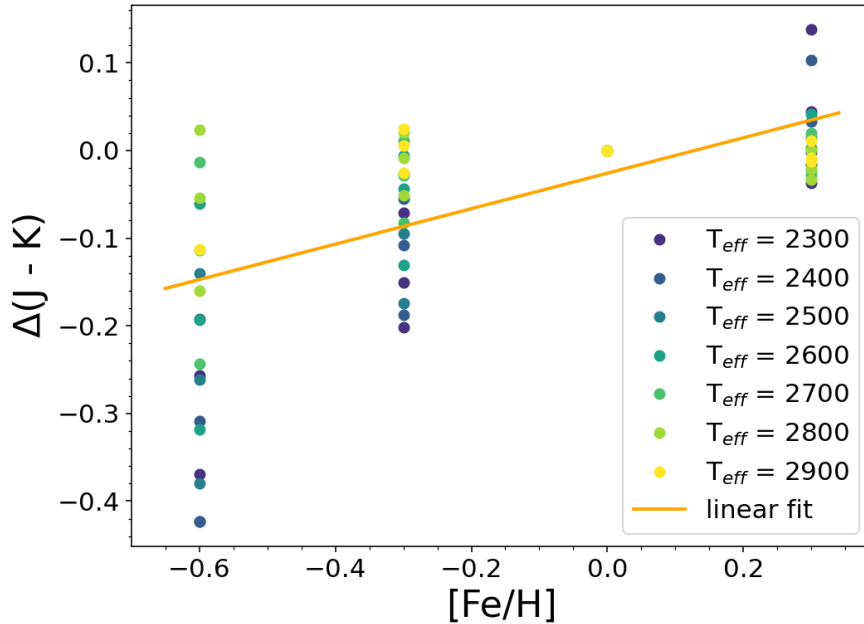


Figure 8. $\Delta(J-K)$ of Drift-Phoenix models calculated with respect to the solar metallicity models as a function of $[Fe/H]$, which serves as a comparison to our observational data in Figure 4. The temperature range is chosen to correspond to field late-M dwarfs. Note that because $\Delta(J-K)$ is calculated with respect to solar metallicity models, so models across all temperatures have $\Delta(J-K)$ of 0 for the solar metallicity models and the points are stacked on top of each other.

with $a = [1.637, -0.2910, 0.022557]$. This relationship is valid for stars with $-0.1 < \Delta(J-K) < 0.1$ and $V-K > 3.8$, and yielded metallicities accurate to ± 0.15 dex based on their sample.

Mann et al. (2013) tested this relationship with a different sample of early- to mid-M dwarfs and found an RMS of 0.20 dex about the fitted relation. In attempt to improve the calibration, their best-fit relation was

$$[Fe/H] = -0.11 + 3.14\Delta(J-K) \quad (2)$$

which slightly improved the RMS to 0.19 dex.

In this work, by rearranging the best-fit relationships in Section 3, we obtain two separate metallicity relations as functions of $\Delta(J-K)$ for late-M dwarfs and L dwarfs. For late-M dwarfs, the relation is

$$[Fe/H]_M = 0.48 + 5.99\Delta(J-K)_M \quad (3)$$

and for L dwarfs, the relation is

$$[Fe/H]_L = 0.03 + 4.90\Delta(J-K)_L. \quad (4)$$

Of course, we define our $\Delta(J-K)$ differently than Johnson et al. (2012), being as the difference between an object's $J-K$ color and the median $J-K$ color of its corresponding SpT (Table 2). The residual error to our fit for the late-M dwarf sample has an RMS of 0.61 dex, and 0.95 dex for L dwarf sample. The large residual errors may be attributed to the fact that metallicity is not the only thing affecting $J-K$ colors of these objects (e.g. viewing geometry and surface gravity as discussed in Section 1), which leads to large scatter in the fitted relations. Inconsistencies of methods that were used for metallicity measurements in different literature that we collected our sample from also serve as a contributor to the errors. Thus, these empirical relationships are not reliable for metallicity measurements for late-M and L dwarfs but may serve as an easy way to obtain crude metallicity information when only the photometry is available.

6. CONCLUSION

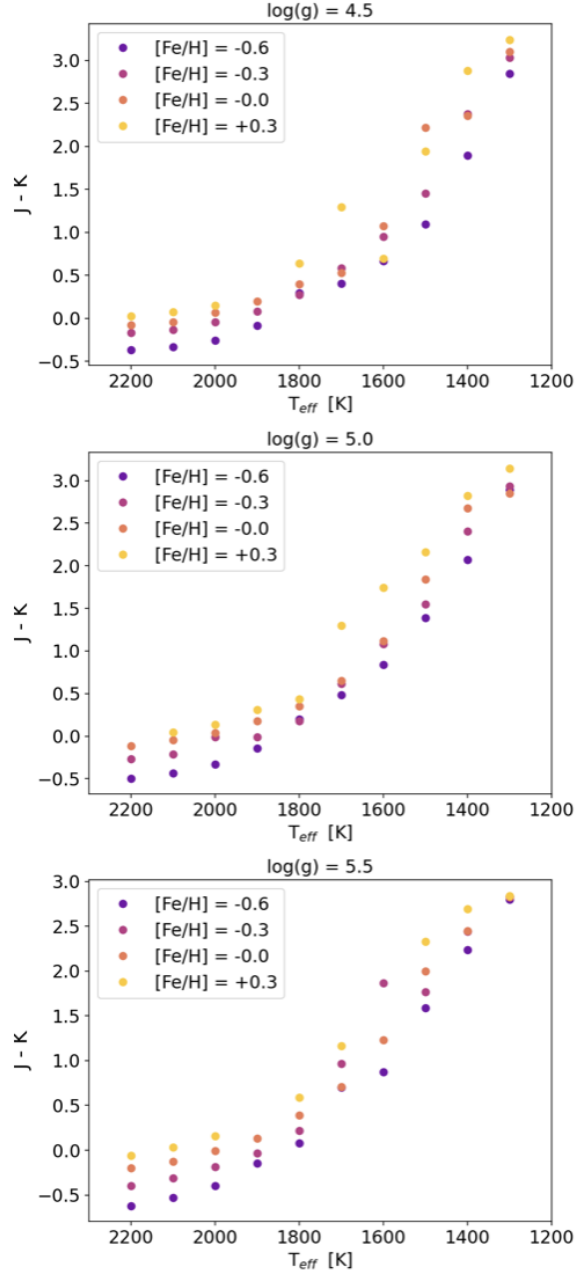


Figure 9. Drift-Phoenix models with a temperature range of [1300 - 2200 K] and a $\log(g)$ range of [4.5, 5.0, 5.5] $\log(\frac{cm}{s^2})$, which corresponds to L dwarfs. All photometry is on the MKO system.

We assembled a sample of 64 ultracool dwarf companions with known metallicities from their primary stars, comprising 32 late-M dwarfs and 32 L dwarfs. This included 6 new ultracool dwarfs that we identified using the binary catalog from El-Badry et al. (2021) and SED fitting. Spearman’s rank correlation test showed that the late-M dwarfs sample (the L dwarfs sample) has a positive correlation with 95% (90%) confidence level between the color anomaly $\Delta(J - K)$ and metallicity. A linear fit to the data gives a slope of 0.17 ± 0.07 ($0.20^{+0.07}_{-0.08}$) and a constant of -0.08 ± 0.01 (-0.01 ± 0.02). The more metal-rich an object is, the redder it appears, which suggests that higher metallicity induces more condensate formation in the atmospheres of these ultracool dwarfs. The Drift-Phoenix models also showed similar trends, but the L dwarf models had a larger slope of 0.49 ± 0.02 . This suggests that the atmosphere models of these

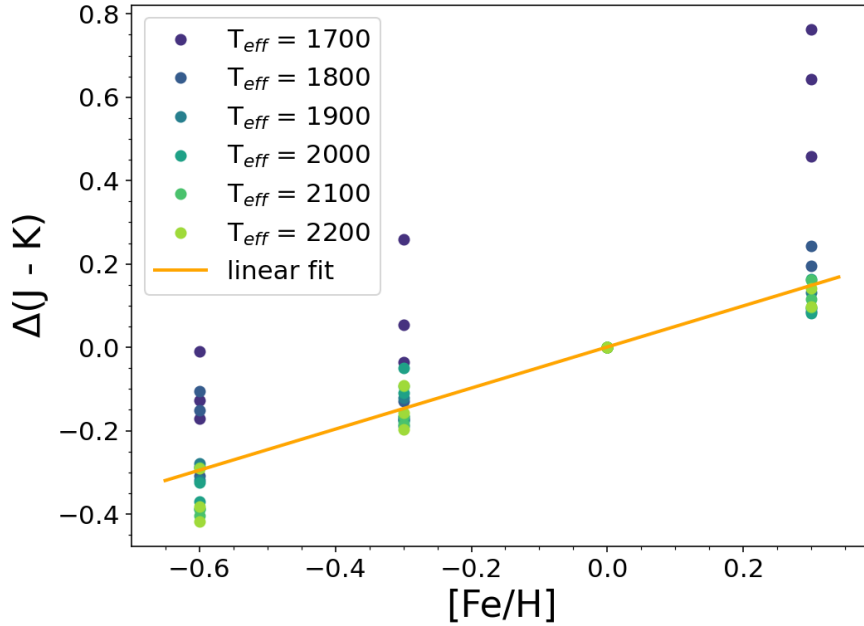


Figure 10. $\Delta(J-K)$ of Drift-Phoenix models calculated with respect to the solar metallicity models as a function of $[\text{Fe}/\text{H}]$, which serves as a comparison to our observational data in Figure 4. The temperature range is chosen to correspond to field L dwarfs. Similar to Figure 8, because $\Delta(J-K)$ is calculated with respect to solar metallicity models, so models across all temperatures have $\Delta(J-K)$ of 0 for the solar metallicity models and the points are stacked on top of each other.

ultracool objects need to be improved to match observational data. We also used 2-sample KS test to confirm that our sample of ultracool dwarfs have consistent metallicity distribution compared to the field FGK stars.

This study serves to provide an observed relationship between $\Delta(J-K)$ color and metallicity for these objects to improve future atmospheric models, thus gain a better and more complete understanding of condensate formation in ultracool dwarf and giant exoplanet atmospheres. We also discuss the possibility to use the empirical relationship to obtain crudely approximated metallicity given a $(J-K)$ color. We may improve and further constrain the relationships found in this work using larger samples of late-M and L dwarfs, such as those that will result from the Legacy Survey of Space and Time (LSST) conducted at Rubin Observatory.

Facilities: Pan-STARRS, UKIRT

Table 1. Fitted polynomial coefficients of ultracool dwarf colors as functions of spectral types

Color	SPT	a ₀	a ₁	a ₂	a ₃	a ₄	a ₅	a ₆	a ₇	a ₈	a ₉
<i>g</i> - <i>W</i> 1	[0, 11]	+4.412E+0	+5.6163E-1	-2.6113E-1	+8.9422E-2	-1.0354E-2	+4.8532E-4	-8.0770E-6			
<i>r</i> - <i>W</i> 1	[0, 16]	+3.228E+0	+3.78073E-1	-4.35955E-2	-1.40900E-2	+1.41348E-2	-2.61549E-3	+1.95128E-4	-6.08834E-6	+5.69910E-8	
<i>i</i> - <i>W</i> 1	[0, 20]	+2.553E+0	+1.38372E-1	+3.74034E-2	-4.76123E-2	+2.06378E-2	-3.72891E-3	+3.46061E-4	-1.74675E-5	+4.57227E-7	-4.87456E-9
<i>z</i> - <i>W</i> 1	[0, 28]	+2.236E+0	+1.82857E-1	-1.39936E-1	+5.37396E-2	-8.44757E-3	+7.12631E-4	-3.42884E-5	+9.18231E-7	-1.22666E-8	+5.89381E-11
<i>y</i> - <i>W</i> 1	[0, 29]	+2.063E+0	+1.29408E-1	-1.10970E-1	+4.42354E-2	-7.69674E-3	+7.41032E-4	-4.13195E-5	+1.311955E-6	-2.189699E-8	+1.487118E-10
<i>J</i> - <i>W</i> 1	[0, 30]	+9.366E-1	+7.36787E-2	-7.03136E-2	+2.81689E-2	-5.05757E-3	+4.90706E-4	-2.66342E-5	+7.964306E-7	-1.213588E-8	+7.292408E-10
<i>H</i> - <i>W</i> 1	[0, 30]	+2.736E-1	+1.08221E-1	-7.95243E-2	+3.05663E-2	-5.51001E-3	+5.46211E-4	-3.11239E-5	+1.011902E-6	-1.747484E-8	+1.249830E-10
<i>K</i> - <i>W</i> 1	[0, 30]	+9.896E-2	+7.51401E-3	+1.67941E-3	+7.78834E-4	-2.80064E-4	+3.45669E-5	-1.87863E-6	+4.539632E-8	-3.906790E-8	
<i>W</i> 1 - <i>W</i> 2	[0, 30]	-2.732E-2	-3.8613E-2	-7.56159E-3	+3.15515E-3	-4.12880E-4	+2.57523E-5	-7.80082E-7	+9.018347E-9		

Table 2. Median $J - K$ colors as a function of SpT calculated from field dwarfs in the UCS

SpT	$J - K$	SpT	$J - K$
6.0	0.979	19.0	1.627
6.5	0.956	19.5	1.376
7.0	1.013	20.0	1.303
7.5	1.021	20.5	1.187
8.0	1.072	21.0	1.071
8.5	1.084	21.5	1.002
9.0	1.149	22.0	0.827
9.5	1.214	22.5	0.649
10.0	1.188	23.0	0.426
10.5	1.222	23.5	0.288
11.0	1.263	24.0	0.135
11.5	1.332	24.5	-0.065
12.0	1.416	25.0	-0.248
12.5	1.456	25.5	-0.246
13.0	1.493	26.0	-0.387
13.5	1.601	26.5	-0.320
14.0	1.497	27.0	-0.282
14.5	1.578	27.5	-0.466
15.0	1.640	28.0	-0.430
15.5	1.713	28.5	-0.387
16.0	1.664	29.0	-0.556
16.5	1.685	29.5	-0.733
17.0	1.764	30.0	-0.910
17.5	1.798		
18.0	1.737		
18.5	1.717		

Table 3. M Dwarfs Sample

Name	RA (J2000)	Dec (J2000)	SpT	J [mag]	K [mag]	$\Delta(J-K)$ [mag]	Primary Star	P-SpT	Sep [as]	Sep [AU]	[Fe/H]	References
HIP 6217C	19.9361	0.1051	9.5; IR	15.402±0.006	14.454±0.008	-0.266±0.010	HIP 6217	G6	27.4	3014.0	0.258±0.09	1, 1, 2, 2, 3
2MASS J03184214+0828002	49.6756	8.4667	7.0; IR	13.647±0.027	12.662±0.023	-0.028±0.035	NLTT 10534	M3	75.5	3098.7	0.19±0.10	4, 4, 5, 5, 4
2MASS J03275437-1107205	51.9767	-11.1223	[7.5]	14.227±0.037	13.319±0.039	-0.113±0.054	UCAC3 158-9098		100.3	5327.0	0.056±0.08	6, 0, 5, 5, 3
2MASS J04095631-2454273	62.4849	-24.9076	[9.5]	15.807±0.085	14.919±0.126	-0.326±0.152	TYC 6456-1296-1		145.3	11706.0	0.163±0.08	6, 0, 5, 5, 3
2MASS J04305157-0849007	67.7149	-8.8169	8.5; IR	12.739±0.022	11.767±0.023	-0.113±0.032	LP 655-23	M4	14.4	450.0	0.030±0.10	7, 4, 5, 5, 4
2MASS J07394386+1305070	114.9327	13.0852	8.0; opt	13.910±0.096	12.773±0.052	0.065±0.109	BD+13 1727	K5	10.5	517.6	0.150±0.03	8, 9, 5, 5, 4
2MASS J08061871+4446586	121.5780	44.7828	[9.0]	15.856±0.067	14.677±0.083	0.030±0.107	2M08061929+4446362		23.2	1955.3	0.069±0.01	6, 0, 5, 5, 10
NLTT19472	126.2143	-3.6836	6.0; IR	11.418±0.026	10.604±0.019	-0.156±0.028	HIP 41211	F6	356.4	9729.7	-0.28±0.08	11, 4, 5, 5, 12
LSPM J0942+2351	145.7283	23.8553	6.5; IR	13.146±0.024	12.257±0.021	-0.067±0.032	NLTT 22411	M1	132.6	4759.6	0.05±0.10	13, 4, 5, 5, 4
HIP 49046B	150.1488	27.2849	6.5; IR	12.930±0.092	12.038±0.021	-0.064±0.094	HIP 49046	M0.5	136.1	4868.3	0.190	1, 1, 1, 5, 14
20 LMi B	150.2091	31.9289	6.0; IR	10.125±0.018	9.243±0.018	-0.088±0.025	HIP 49081	G3	158.2	2357.2	0.200±0.03	1, 4, 5, 5, 4
PM 111055+4331	166.3788	43.5214	6.5; IR	8.602±0.026	7.810±0.026	-0.164±0.037	HIP 54211	M1	31.4	154.0	-0.32±0.10	4, 4, 5, 5, 4
NLTT28453	176.3975	-20.3511	6.0; IR	11.597±0.026	10.745±0.023	-0.118±0.028	HIP 57361	M2.5	15.4	297.9	-0.05±0.10	1, 4, 5, 5, 4
2MASS J12003292+2048513	180.1371	20.8143	7.0; opt	12.862±0.021	11.861±0.022	-0.012±0.030	G 121-42	M3	204.0	5022.5	-0.130	15, 15, 5, 5, 16
HIP 59310B	182.5412	18.9690	7.0; IR	13.672±0.027	12.676±0.024	-0.017±0.036	HIP 59310	K3	82.1	3735.5	0.30±0.03	1, 1, 17, 17, 18
NLTT 30510B	185.5767	36.7302	9.5; IR	15.923±0.080	14.826±0.090	-0.116±0.120	NLTT 30510		19.6	1352.4	-0.60±0.02	1, 1, 17, 17, 10
2MASS J13204159+0957506	200.1733	9.9639	7.0; IR	13.650±0.010	12.584±0.029	0.053±0.031	HIP 65133	K2	168.0	6078.5	0.07±0.03	19, 4, 20, 5, 4
HIP 65706B	202.0872	30.0552	7.0; IR	13.246±0.021	12.258±0.002	-0.025±0.002	HIP 65706	K5	52.6	2227.6	0.114±0.01	1, 1, 2, 2, 11
NLTT 36549	213.0505	-0.5878	7.5; IR	12.943±0.004	12.066±0.026	-0.144±0.035	NLTT 36548	M3.5	12.0	3221.6	-0.26±0.10	21, 4, 5, 5, 4
G1 569 B	223.6226	16.1024	8.5; opt	10.750±0.060	9.620±0.030	0.046±0.067	G1 569 A	M3	5.0	49.7	0.230±0.04	22, 23, 24, 24, 25
2MASS J15303823+3027153	232.6586	30.4540	[9.0]	15.520±0.010	14.373±0.008	-0.0026±0.013	2M15304088+3027059	K5	35.5	2865.5	0.198±0.01	6, 0, 26, 27, 10
2MASS J15575669+5914232	239.4821	59.2398	9.0; IR	14.156±0.031	13.120±0.030	-0.113±0.043	HIP 78184	K5	119.0	3871.0	0.080±0.10	7, 28, 5, 5, 4
HIP 78916B	241.6345	22.8927	8.0; IR	15.148±0.018	14.172±0.053	-0.096±0.056	HIP 78916	G0	35.5	3035.2	-0.005±0.01	1, 1, 1, 17, 10
HIP 81910B	250.9563	-26.8109	6.0; IR	12.400±0.010	11.505±0.025	-0.075±0.027	HIP 81910	G2.5	26.7	1254.1	0.183±0.02	1, 1, 1, 17, 29
vB 8	253.8970	-8.3944	7.0; opt	9.632±0.029	8.791±0.023	-0.172±0.037	LSPM J1717+5925	M3.5	231.0	1500.3	-0.16±0.09	30, 30, 5, 5, 31
LSPM J1717+5925B	259.3792	59.4254	9.0; IR	16.509±0.018	15.195±0.054	0.165±0.057	LSPM J1717+5925	G6	14.4	1762.6	0.250±0.00	1, 1, 1, 17, 10
vB 10	289.2400	5.1504	7.5; IR	9.760±0.025	8.745±0.022	-0.0061±0.033	HIP 94761	M3	75.2	443.7	0.110±0.10	32, 4, 5, 5, 4
2MASS J20103539+0634367	302.6475	6.5767	9.0; IR	12.389±0.024	11.423±0.021	-0.183±0.032	NLTT 48838	M4	142.8	2313.4	-0.010±0.10	33, 4, 5, 5, 4
LSPM J2049+3216W	312.3073	32.2808	6.0; IR	11.633±0.023	10.829±0.019	-0.166±0.030	HIP 102766	K2.5	34.4	801.5	-0.020±0.03	4, 4, 5, 5, 4
LSPM J2153+1157B	328.4458	11.9633	7.0; IR	14.450±0.011	13.368±0.011	0.069±0.016	LSPM J2153+1157		11.3	601.2	-0.112±0.01	1, 1, 1, 1, 10
2MASS J22264440-7503425	336.6851	-75.0618	8.0; opt	12.353±0.023	11.246±0.023	0.035±0.033	HD 212168	G0	265.0	6222.2	0.020±0.03	34, 19, 5, 5, 35
G 216-7B	339.3856	39.3775	9.5; opt	13.173±0.022	12.183±0.019	-0.224±0.030	HIP 111685	M0	33.6	705.2	0.030±0.10	36, 36, 5, 5, 4

NOTE—2MASS J00034227-2822410 was considered for the sample, but it was not included due to its higher luminosity (by > 2 σ) compared to the field ultracool dwarfs of the same spectral type, suggesting that it might be a young object. The numbering for the spectral types follows the ultracool dwarfs convention such that M6 is labeled as 6.0, M7 is 7.0, so on and so forth. The type of SpT, whether it be optical or IR, is indicated with either the 'opt' flag or the 'IR' flag. Objects with spectral types with brackets around them are new benchmark objects we identified in this work. Spectral types are estimated from our SED fitting procedure. 'P-SpT' stands for primary star SpT. Reference format: first number is the discovery reference, second is the SpT reference, third and fourth are the J and K photometry reference, and the last number is the metallicity reference. References: 0 = this work, 1 = Deacon et al. (2014), 2 = Lawrence et al. (2012), 3 = Steinmetz et al. (2020), 4 = Mann et al. (2014), 5 = Cutri et al. (2003), 6 = El-Badry et al. (2021), 7 = Cruz et al. (2003), 8 = Lépine et al. (2002), 9 = Cruz et al. (2007), 10 = Majewski et al. (2017), 11 = Allen et al. (2012), 12 = Casagrande et al. (2011), 13 = West et al. (2011), 14 = Gaias et al. (2014), 15 = Gaias et al. (2009), 16 = Newton et al. (2014), 17 = Best et al. (2020a), 18 = Grievens et al. (2018), 19 = Reid et al. (2008), 20 = Smith et al. (2014), 21 = Bessell (1991), 22 = Skrutskie et al. (1987), 23 = Henry & Kirkpatrick (1990), 24 = Dupuy et al. (2010), 25 = Hinkel et al. (2014), 26 = Dye et al. (2018), 27 = Dahm et al. (2013), 28 = Thompson et al. (2013), 29 = Liu et al. (2020), 30 = Henry et al. (2004), 31 = Kuznetsov et al. (2019), 32 = Kirkpatrick et al. (1991), 33 = Luhman et al. (1991), 34 = Luhman et al. (2012), 35 = Luhman (1979), 36 = Ghezzi et al. (2007). All parallax related information comes from Gaia Collaboration et al. (2018) and Gaia Collaboration et al. (2021).

Table 4. L Dwarfs Sample

Name	RA (J2000)	Dec (J2000)	SpT	J [mag]	K [mag]	$\Delta(J-K)$ [mag]	Primary Star	P-SpT	Sep [as]	Sep [AU]	[Fe/H]	References
LHS 102B	1.1453	-40.7351	15.0; opt	13.060±0.030	11.360±0.030	0.060±0.042	GJ 1001A	M4	18.6	226.5	-0.060±0.09	39, 37, 38, 38, 31
NLTT 1011B	4.8865	40.3159	12.0; IR	15.485±0.059	14.299±0.066	-0.230±0.089	NLTT 1011		58.5	3276.0	-0.048±0.39	1, 1, 17, 17, 40
HIP 2397B	7.6033	22.7469	10.5; IR	14.552±0.012	13.370±0.052	-0.040±0.053	HIP 2397	K2	117.1	4063.4	-0.220±0.09	1, 1, 1, 17, 41
HD 3861B	10.2945	9.3556	13.5; IR	15.690±0.006	13.988±0.006	0.101±0.003	HD 3861A	F8	16.5	554.2	0.137±0.01	42, 42, 2, 2, 25
HIP 6407B	20.5707	3.5232	11.0; IR	15.345±0.005	14.203±0.006	-0.121±0.008	HIP 6407 / NLTT 4558	G5	44.9	2105.8	-0.020±0.03	1, 1, 2, 2, 25
HIP 9269B	29.7950	33.2087	16.0; IR	16.126±0.017	14.298±0.019	0.165±0.025	HIP 9269	G9	52.1	1290.3	0.280±0.06	1, 1, 1, 1, 25
SDSS J020735.60+135556.3	31.8983	13.9323	13.0; opt	15.369±0.005	13.829±0.005	0.047±0.007	G 3-40	M2	72.5	2697.0	0.118±0.01	43, 43, 2, 2, 10
GJ 1048B	38.9997	-23.5223	11.0; IR	13.660±0.500	12.170±0.080	0.227±0.506	GJ 1048A	K3.5	11.9	256.4	0.070±0.09	44, 44, 45, 45, 25
HIP 26653B	84.9564	52.8999	11.5; IR	14.670±0.020	13.298±0.029	0.040±0.035	HIP 26653	G5	27.0	747.9	-0.010±0.12	1, 1, 46, 17, 25
LSPM J0632+5053B	98.2021	50.8931	11.5; IR	16.612±0.027	15.172±0.058	0.108±0.064	LSPM J0632+5053		47.4	4029.0	0.050	1, 1, 1, 17, 47
HD 46588B	101.6120	79.5835	19.0; IR	16.097±0.093	14.600±0.090	-0.130±0.129	HD 46588A	F7	79.2	1441.4	-0.085±0.13	48, 48, 5, 5, 25
2MASS J07481084-2731309	117.0448	-27.5251	[10.0]	16.024±0.098	14.945±0.149	-0.109±0.178	HD 6348A	G2	72.2	5224.0	0.075	6, 0, 5, 5, 49
eta Cnc B	128.1325	20.4502	13.0; IR	17.737±0.035	16.523±0.036	-0.279±0.050	eta Cnc A	K3	164.0	15530.8	0.145±0.04	50, 50, 2, 2, 25
SDSS J085836.98+271050.8	134.6539	27.1810	10.0; opt	15.011±0.003	13.594±0.004	0.229±0.005	LP 312-49 / NLTT 20640	M4	15.4	816.2	-0.133±0.02	51, 51, 2, 2, 10
HD 89744B	155.5620	41.2407	10.0; opt	14.850±0.040	13.580±0.040	0.082±0.057	HD 89744A	F7	63.1	2429.3	0.235±0.09	52, 52, 53, 53, 25
GJ 417B	168.1068	35.8035	14.5; opt	14.470±0.020	12.670±0.030	0.222±0.036	GJ 417A	G2	90.0	2097.0	0.115±0.03	54, 54, 46, 45, 25
NLTT 27966B	174.1654	48.8778	14.0; IR	16.106±0.019	14.669±0.054	-0.060±0.057	NLTT 27966	F8	15.9	833.3	-0.440±0.03	1, 1, 1, 17, 25
HIP 59933B	184.4020	14.4534	11.0; IR	15.995±0.008	14.620±0.010	0.112±0.013	HIP 59933		38.1	2560.3	0.140±0.04	1, 1, 2, 2, 41
LSPM J1336+2541B	204.1043	25.6769	14.0; IR	16.935±0.017	15.478±0.016	-0.040±0.023	LSPM J1336+2541		121.7	9582.7	-0.483±0.02	1, 1, 2, 2, 10
2MASS J13475911-7610054	206.9960	-76.1681	10.0; opt	13.671±0.033	12.554±0.032	-0.071±0.046	2MASS J13475680-7610199	M1	16.8	525.8	-0.478±0.08	55, 56, 5, 5, 3
PM 113518+4157B	207.9478	41.9633	11.5; IR	15.018±0.032	13.837±0.040	-0.151±0.051	PM 113518+4157		21.6	1013.0	0.061±0.01	1, 1, 17, 17, 25
G 239-25B	220.5919	66.0555	10.0; IR	11.440±0.030	10.300±0.070	-0.048±0.076	G 239-25A	M3	2.9	31.7	-0.240±0.04	57, 58, 45, 45, 25
HD 130948B	222.5667	23.9116	14.0; IR	13.200±0.080	11.690±0.040	0.013±0.089	HD 130948A	F9	2.6	48.1	-0.010±0.12	59, 60, 61, 61, 25
HIP 73169B	224.2985	-6.3240	12.5; IR	15.929±0.020	14.446±0.016	0.027±0.026	HIP 73169	M0	29.1	1307.8	-0.010	1, 1, 1, 1, 15
beta Cir B	229.3400	-58.8583	11.0; IR	14.408±0.004	13.196±0.043	-0.051±0.043	beta Cir	A3	216.0	6199.2	0.200	62, 62, 63, 5, 64
GJ 584C	230.8443	30.2489	18.0; opt	16.082±0.007	14.376±0.007	-0.061±0.010	GJ 584AB	G2+G2	194.0	3464.8	-0.010±0.04	54, 54, 2, 2, 25
GJ 618.1B	245.1090	-4.2755	12.5; opt	15.180±0.050	13.550±0.040	0.174±0.064	GJ 618.1A	K7	35.9	1166.7	0.370±0.09	52, 52, 45, 45, 31
FSO J259.4554+29.9198	259.4554	29.9199	[13.5]	15.875±0.014	14.488±0.022	-0.215±0.026	2MASS J17174844+2955095		11.6	710.1	0.019±0.01	6, 0, 26, 27, 10
LTT 7251B	273.9548	-23.8126	17.0; IR	16.930±0.090	15.445±0.090	-0.280±0.103	LTT 7251	G8	14.7	554.8	-0.150±0.04	65, 65, 65, 65, 25
zeta Del B	308.8294	14.6710	15.0; IR	17.180±0.090	15.400±0.070	0.140±0.114	zeta Del	A3	13.5	903.1	-0.050	66, 66, 66, 66, 64
SDSS J213154.43-011939.3	322.9770	-1.3273	19.0; opt	17.230±0.015	15.545±0.210	0.058±0.211	NLTT 51469AB	M3+M6	83.0	3859.5	-0.411±0.02	67, 68, 68, 17, 10
HD 221356D	352.8791	-4.0897	11.0; IR	13.763±0.038	12.755±0.025	-0.255±0.045	HD 221356ABC	F7+M8+L3	12.1	315.0	-0.190±0.06	69, 69, 69, 69, 25

NOTE—L dwarfs spectral types starts at L0 = 10.0, continuing after the M spectral types. The reference format follows Table 3. The indexing of the references is the same as Table 3 for repeated references. The references not listed under Table 3 are listed below.
References: 37 = Kirkpatrick et al. (2001), 38 = Leggett et al. (2010), 39 = EROS Collaboration et al. (1999), 40 = Cui et al. (2012), 41 = Kiefer et al. (2019), 42 = Scholz (2016), 43 = Hawley et al. (2002), 44 = Gizis et al. (2001), 45 = Faherty et al. (2012), 46 = Best et al. (2020b), 47 = Bochanski et al. (2018), 48 = Loutrel et al. (2011), 49 = Casali et al. (2020), 50 = Zhang et al. (2010), 51 = West et al. (2008), 52 = Wilson et al. (2001), 53 = Dupuy & Liu (2012), 54 = Kirkpatrick et al. (2000), 55 = Kendall et al. (2007), 56 = Pihan-Bao et al. (2008), 57 = Gollinowski et al. (2004), 58 = Forveille et al. (2004), 59 = Porter et al. (2002), 60 = Goto et al. (2002), 61 = Dupuy et al. (2009), 62 = Smith et al. (2015), 63 = Minniti et al. (2017), 64 = Erspanner & North (2003), 65 = Smith et al. (2018), 66 = De Rosa et al. (2014), 67 = Chiu et al. (2006), 68 = Gauza et al. (2019), 69 = Gauza et al. (2012).

ACKNOWLEDGMENTS

This work has benefited from The UltracoolSheet at <http://bit.ly/UltracoolSheet>, maintained by Will Best, Trent Dupuy, Michael Liu, Rob Siverd, and Zhoujian Zhang, and developed from compilations by Dupuy & Liu (2012), Dupuy & Kraus (2013), Liu et al. (2016), Best et al. (2018b), and Best et al. (2020a). We would like to give a special thanks to Eugene Magnier, Robert Siverd, Jamie Tayar, Zachary Claytor, and Ryan Dungee for helpful discussions regarding data analysis. The Pan-STARRS1 Surveys (PS1) and the PS1 public science archive have been made possible through contributions by the Institute for Astronomy, the University of Hawaii, the Pan-STARRS Project Office, the Max-Planck Society and its participating institutes, the Max Planck Institute for Astronomy, Heidelberg and the Max Planck Institute for Extraterrestrial Physics, Garching, The Johns Hopkins University, Durham University, the University of Edinburgh, the Queen’s University Belfast, the Harvard-Smithsonian Center for Astrophysics, the Las Cumbres Observatory Global Telescope Network Incorporated, the National Central University of Taiwan, the Space Telescope Science Institute, the National Aeronautics and Space Administration under Grant No. NNX08AR22G issued through the Planetary Science Division of the NASA Science Mission Directorate, the National Science Foundation Grant No. AST-1238877, the University of Maryland, Eotvos Lorand University (ELTE), the Los Alamos National Laboratory, and the Gordon and Betty Moore Foundation. This publication makes use of data products from the Two Micron All Sky Survey, which is a joint project of the University of Massachusetts and the Infrared Processing and Analysis Center/California Institute of Technology, funded by the National Aeronautics and Space Administration and the National Science Foundation. This research has made use of the SIMBAD database and NASA/IPAC Infrared Science Archive. The UKIDSS project is defined in Lawrence et al. 2007. UKIDSS uses the UKIRT Wide Field Camera (WFCAM; Casali et al. 2007) and a photometric system described in Hewett et al. 2006. The pipeline processing and science archive are described in Irwin et al. (2004) and Hambly et al. (2008). The UHS is a partnership between the UK STFC, The University of Hawaii, The University of Arizona, Lockheed Martin and NASA. We have used data from the J-band data release described in detail in Dye et al. (2018) and the K-band data release described in Dahm et al. (2018). Some data in this work were obtained on Maunakea, the authors wish to recognize and acknowledge the very significant cultural role and reverence that the summit of Maunakea has always had within the indigenous Hawaiian community. We are most fortunate to have the opportunity to conduct observations from this mountain.

REFERENCES

- Allard, F. 2014, in *Exploring the Formation and Evolution of Planetary Systems*, ed. M. Booth, B. C. Matthews, & J. R. Graham, Vol. 299, 271–272, doi: [10.1017/S1743921313008545](https://doi.org/10.1017/S1743921313008545)
- Allard, F., Homeier, D., & Freytag, B. 2011, in *Astronomical Society of the Pacific Conference Series*, Vol. 448, 16th Cambridge Workshop on Cool Stars, Stellar Systems, and the Sun, ed. C. Johns-Krull, M. K. Browning, & A. A. West, 91. <https://arxiv.org/abs/1011.5405>
- Allen, P. R., Burgasser, A. J., Faherty, J. K., & Kirkpatrick, J. D. 2012, *AJ*, 144, 62, doi: [10.1088/0004-6256/144/2/62](https://doi.org/10.1088/0004-6256/144/2/62)
- Asplund, M., Grevesse, N., & Sauval, A. J. 2005, in *Astronomical Society of the Pacific Conference Series*, Vol. 336, *Cosmic Abundances as Records of Stellar Evolution and Nucleosynthesis*, ed. I. Barnes, Thomas G. & F. N. Bash, 25
- Baron, E., Hauschildt, P. H., Allard, F., et al. 2003, in *Modelling of Stellar Atmospheres*, ed. N. Piskunov, W. W. Weiss, & D. F. Gray, Vol. 210, 19, doi: [10.48550/arXiv.astro-ph/0209052](https://doi.org/10.48550/arXiv.astro-ph/0209052)
- Bessell, M. S. 1991, *AJ*, 101, 662, doi: [10.1086/115714](https://doi.org/10.1086/115714)
- Best, W. M. J., Dupuy, T. J., Liu, M. C., Siverd, R. J., & Zhang, Z. 2020, Zenodo, doi: [10.5281/zenodo.4169085](https://doi.org/10.5281/zenodo.4169085)
- Best, W. M. J., Liu, M. C., Magnier, E. A., & Dupuy, T. J. 2020a, *AJ*, 159, 257, doi: [10.3847/1538-3881/ab84f4](https://doi.org/10.3847/1538-3881/ab84f4)
- . 2020b, *AJ*, 159, 257, doi: [10.3847/1538-3881/ab84f4](https://doi.org/10.3847/1538-3881/ab84f4)
- Best, W. M. J., Magnier, E. A., Liu, M. C., et al. 2018a, *VizieR Online Data Catalog*, *J/ApJS/234/1*
- Best, W. M. J., Magnier, E. A., Liu, M. C., et al. 2018b, *ApJS*, 234, 1, doi: [10.3847/1538-4365/aa9982](https://doi.org/10.3847/1538-4365/aa9982)
- Bochanski, J. J., Faherty, J. K., Gagné, J., et al. 2018, *AJ*, 155, 149, doi: [10.3847/1538-3881/aaeabe](https://doi.org/10.3847/1538-3881/aaeabe)
- Boggs, P. T., Spiegelman, C. H., Donaldson, J. R., & Schnabel, R. B. 1988, *Journal of Econometrics*, 38, 169, doi: [https://doi.org/10.1016/0304-4076\(88\)90032-2](https://doi.org/10.1016/0304-4076(88)90032-2)
- Burrows, A., Hubbard, W. B., Lunine, J. I., & Liebert, J. 2001, *Reviews of Modern Physics*, 73, 719, doi: [10.1103/RevModPhys.73.719](https://doi.org/10.1103/RevModPhys.73.719)
- Burrows, A., & Sharp, C. M. 1999, *ApJ*, 512, 843, doi: [10.1086/306811](https://doi.org/10.1086/306811)
- Casagrande, L., Schönrich, R., Asplund, M., et al. 2011, *A&A*, 530, A138, doi: [10.1051/0004-6361/201016276](https://doi.org/10.1051/0004-6361/201016276)

- Casali, G., Spina, L., Magrini, L., et al. 2020, *A&A*, 639, A127, doi: [10.1051/0004-6361/202038055](https://doi.org/10.1051/0004-6361/202038055)
- Casali, M., Adamson, A., Alves de Oliveira, C., et al. 2007, *A&A*, 467, 777, doi: [10.1051/0004-6361:20066514](https://doi.org/10.1051/0004-6361:20066514)
- Chambers, K. C., Magnier, E. A., Metcalfe, N., et al. 2016, arXiv e-prints, arXiv:1612.05560, <https://arxiv.org/abs/1612.05560>
- Chiu, K., Fan, X., Leggett, S. K., et al. 2006, *AJ*, 131, 2722, doi: [10.1086/501431](https://doi.org/10.1086/501431)
- Cruz, K. L., Reid, I. N., Liebert, J., Kirkpatrick, J. D., & Lowrance, P. J. 2003, *AJ*, 126, 2421, doi: [10.1086/378607](https://doi.org/10.1086/378607)
- Cruz, K. L., Reid, I. N., Kirkpatrick, J. D., et al. 2007, *AJ*, 133, 439, doi: [10.1086/510132](https://doi.org/10.1086/510132)
- Cui, X.-Q., Zhao, Y.-H., Chu, Y.-Q., et al. 2012, *Research in Astronomy and Astrophysics*, 12, 1197, doi: [10.1088/1674-4527/12/9/003](https://doi.org/10.1088/1674-4527/12/9/003)
- Cutri, R. M., Skrutskie, M. F., van Dyk, S., et al. 2003, 2MASS All Sky Catalog of point sources. (SAO/NASA)
- Dahm, S., Bruursema, J., Munn, J. A., et al. 2018, in *American Astronomical Society Meeting Abstracts*, Vol. 231, American Astronomical Society Meeting Abstracts #231, 436.04
- De Rosa, R. J., Patience, J., Ward-Duong, K., et al. 2014, *MNRAS*, 445, 3694, doi: [10.1093/mnras/stu2018](https://doi.org/10.1093/mnras/stu2018)
- Deacon, N. R., Liu, M. C., Magnier, E. A., et al. 2014, *ApJ*, 792, 119, doi: [10.1088/0004-637X/792/2/119](https://doi.org/10.1088/0004-637X/792/2/119)
- Dehn, M., Helling, C., Woitke, P., & Hauschildt, P. 2007, in *Convection in Astrophysics*, ed. F. Kupka, I. Roxburgh, & K. L. Chan, Vol. 239, 227–229, doi: [10.1017/S1743921307000488](https://doi.org/10.1017/S1743921307000488)
- Dupuy, T. J., & Kraus, A. L. 2013, *Science*, 341, 1492, doi: [10.1126/science.1241917](https://doi.org/10.1126/science.1241917)
- Dupuy, T. J., & Liu, M. C. 2012, *ApJS*, 201, 19, doi: [10.1088/0067-0049/201/2/19](https://doi.org/10.1088/0067-0049/201/2/19)
- . 2017, *ApJS*, 231, 15, doi: [10.3847/1538-4365/aa5e4c](https://doi.org/10.3847/1538-4365/aa5e4c)
- Dupuy, T. J., Liu, M. C., Bowler, B. P., et al. 2010, *ApJ*, 721, 1725, doi: [10.1088/0004-637X/721/2/1725](https://doi.org/10.1088/0004-637X/721/2/1725)
- Dupuy, T. J., Liu, M. C., & Ireland, M. J. 2009, *ApJ*, 692, 729, doi: [10.1088/0004-637X/692/1/729](https://doi.org/10.1088/0004-637X/692/1/729)
- Dye, S., Lawrence, A., Read, M. A., et al. 2018, *MNRAS*, 473, 5113, doi: [10.1093/mnras/stx2622](https://doi.org/10.1093/mnras/stx2622)
- El-Badry, K., Rix, H.-W., & Heintz, T. M. 2021, *MNRAS*, 506, 2269, doi: [10.1093/mnras/stab323](https://doi.org/10.1093/mnras/stab323)
- EROS Collaboration, Goldman, B., Delfosse, X., et al. 1999, *A&A*, 351, L5, doi: [10.48550/arXiv.astro-ph/9905162](https://doi.org/10.48550/arXiv.astro-ph/9905162)
- Erspamer, D., & North, P. 2003, *A&A*, 398, 1121, doi: [10.1051/0004-6361:20021711](https://doi.org/10.1051/0004-6361:20021711)
- Faherty, J. K., Burgasser, A. J., Walter, F. M., et al. 2012, *ApJ*, 752, 56, doi: [10.1088/0004-637X/752/1/56](https://doi.org/10.1088/0004-637X/752/1/56)
- Fortney, J. J., Marley, M. S., Saumon, D., & Lodders, K. 2008, *ApJ*, 683, 1104, doi: [10.1086/589942](https://doi.org/10.1086/589942)
- Forveille, T., Ségransan, D., Delorme, P., et al. 2004, *A&A*, 427, L1, doi: [10.1051/0004-6361:200400069](https://doi.org/10.1051/0004-6361:200400069)
- Gaia Collaboration, Brown, A. G. A., Vallenari, A., et al. 2018, *A&A*, 616, A1, doi: [10.1051/0004-6361/201833051](https://doi.org/10.1051/0004-6361/201833051)
- Gaia Collaboration, Brown, A. G. A., Vallenari, A., et al. 2021, *A&A*, 649, A1, doi: [10.1051/0004-6361/202039657](https://doi.org/10.1051/0004-6361/202039657)
- Gaidos, E., Mann, A. W., Lépine, S., et al. 2014, *MNRAS*, 443, 2561, doi: [10.1093/mnras/stu1313](https://doi.org/10.1093/mnras/stu1313)
- García Pérez, A. E., Allende Prieto, C., Holtzman, J. A., et al. 2016, *AJ*, 151, 144, doi: [10.3847/0004-6256/151/6/144](https://doi.org/10.3847/0004-6256/151/6/144)
- Gauza, B., Béjar, V. J. S., Rebolo, R., et al. 2012, *MNRAS*, 427, 2457, doi: [10.1111/j.1365-2966.2012.22113.x](https://doi.org/10.1111/j.1365-2966.2012.22113.x)
- Gauza, B., Béjar, V. J. S., Pérez-Garrido, A., et al. 2019, *MNRAS*, 487, 1149, doi: [10.1093/mnras/stz1284](https://doi.org/10.1093/mnras/stz1284)
- Ghezzi, L., Cunha, K., Smith, V. V., et al. 2010, *ApJ*, 720, 1290, doi: [10.1088/0004-637X/720/2/1290](https://doi.org/10.1088/0004-637X/720/2/1290)
- Gizis, J. E., Kirkpatrick, J. D., & Wilson, J. C. 2001, *AJ*, 121, 2185, doi: [10.1086/319937](https://doi.org/10.1086/319937)
- Gizis, J. E., Monet, D. G., Reid, I. N., et al. 2000, *AJ*, 120, 1085, doi: [10.1086/301456](https://doi.org/10.1086/301456)
- Golimowski, D. A., Henry, T. J., Krist, J. E., et al. 2004, *AJ*, 128, 1733, doi: [10.1086/423911](https://doi.org/10.1086/423911)
- Goto, M., Kobayashi, N., Terada, H., et al. 2002, *ApJL*, 567, L59, doi: [10.1086/339800](https://doi.org/10.1086/339800)
- Grievies, N., Ge, J., Thomas, N., et al. 2018, *MNRAS*, 481, 3244, doi: [10.1093/mnras/sty2431](https://doi.org/10.1093/mnras/sty2431)
- Hambly, N. C., Collins, R. S., Cross, N. J. G., et al. 2008, *MNRAS*, 384, 637, doi: [10.1111/j.1365-2966.2007.12700.x](https://doi.org/10.1111/j.1365-2966.2007.12700.x)
- Hauschildt, P. H., & Baron, E. 1999, *Journal of Computational and Applied Mathematics*, 109, 41, doi: [10.48550/arXiv.astro-ph/9808182](https://doi.org/10.48550/arXiv.astro-ph/9808182)
- Hawley, S. L., Covey, K. R., Knapp, G. R., et al. 2002, *AJ*, 123, 3409, doi: [10.1086/340697](https://doi.org/10.1086/340697)
- Helling, C., Dehn, M., Woitke, P., & Hauschildt, P. H. 2008a, *ApJL*, 675, L105, doi: [10.1086/53346210.48550/arXiv.0801.3733](https://doi.org/10.1086/53346210.48550/arXiv.0801.3733)
- Helling, C., & Woitke, P. 2006, *A&A*, 455, 325, doi: [10.1051/0004-6361:20054598](https://doi.org/10.1051/0004-6361:20054598)
- Helling, C., Woitke, P., & Thi, W. F. 2008b, *A&A*, 485, 547, doi: [10.1051/0004-6361:20078220](https://doi.org/10.1051/0004-6361:20078220)
- Henry, T. J., & Kirkpatrick, J. D. 1990, *ApJL*, 354, L29, doi: [10.1086/185715](https://doi.org/10.1086/185715)
- Henry, T. J., Subasavage, J. P., Brown, M. A., et al. 2004, *AJ*, 128, 2460, doi: [10.1086/425052](https://doi.org/10.1086/425052)
- Hewett, P. C., Warren, S. J., Leggett, S. K., & Hodgkin, S. T. 2006, *MNRAS*, 367, 454, doi: [10.1111/j.1365-2966.2005.09969.x](https://doi.org/10.1111/j.1365-2966.2005.09969.x)

- Hinkel, N. R., Timmes, F. X., Young, P. A., Pagano, M. D., & Turnbull, M. C. 2014, *AJ*, 148, 54, doi: [10.1088/0004-6256/148/3/54](https://doi.org/10.1088/0004-6256/148/3/54)
- Hood, C. E., Fortney, J. J., Line, M. R., & Faherty, J. K. 2023, *ApJ*, 953, 170, doi: [10.3847/1538-4357/ace32e](https://doi.org/10.3847/1538-4357/ace32e)
- Irwin, M. J., Lewis, J., Hodgkin, S., et al. 2004, in *Society of Photo-Optical Instrumentation Engineers (SPIE) Conference Series*, Vol. 5493, *Optimizing Scientific Return for Astronomy through Information Technologies*, ed. P. J. Quinn & A. Bridger, 411–422, doi: [10.1117/12.551449](https://doi.org/10.1117/12.551449)
- Johnson, J. A., Gazak, J. Z., Apps, K., et al. 2012, *AJ*, 143, 111, doi: [10.1088/0004-6256/143/5/111](https://doi.org/10.1088/0004-6256/143/5/111)
- Kendall, T. R., Jones, H. R. A., Pinfield, D. J., et al. 2007, *MNRAS*, 374, 445, doi: [10.1111/j.1365-2966.2006.11026.x](https://doi.org/10.1111/j.1365-2966.2006.11026.x)
- Kiefer, F., Hébrard, G., Sahlmann, J., et al. 2019, *A&A*, 631, A125, doi: [10.1051/0004-6361/201935113](https://doi.org/10.1051/0004-6361/201935113)
- Kirkpatrick, J. D., Dahn, C. C., Monet, D. G., et al. 2001, *AJ*, 121, 3235, doi: [10.1086/321085](https://doi.org/10.1086/321085)
- Kirkpatrick, J. D., Henry, T. J., & McCarthy, Donald W., J. 1991, *ApJS*, 77, 417, doi: [10.1086/191611](https://doi.org/10.1086/191611)
- Kirkpatrick, J. D., Reid, I. N., Liebert, J., et al. 2000, *AJ*, 120, 447, doi: [10.1086/301427](https://doi.org/10.1086/301427)
- Knapp, G. R., Leggett, S. K., Fan, X., et al. 2004, *AJ*, 127, 3553, doi: [10.1086/420707](https://doi.org/10.1086/420707)
- Kuznetsov, M. K., del Burgo, C., Pavlenko, Y. V., & Frith, J. 2019, *ApJ*, 878, 134, doi: [10.3847/1538-4357/ab1fe9](https://doi.org/10.3847/1538-4357/ab1fe9)
- Lacy, B., & Burrows, A. 2023, *ApJ*, 950, 8, doi: [10.3847/1538-4357/acc8cb](https://doi.org/10.3847/1538-4357/acc8cb)
- Lawrence, A., Warren, S. J., Almaini, O., et al. 2007, *MNRAS*, 379, 1599, doi: [10.1111/j.1365-2966.2007.12040.x](https://doi.org/10.1111/j.1365-2966.2007.12040.x)
- . 2012, *VizieR Online Data Catalog*, II/314
- Leggett, S. K. 1992, *ApJS*, 82, 351, doi: [10.1086/191720](https://doi.org/10.1086/191720)
- Leggett, S. K., Burningham, B., Saumon, D., et al. 2010, *ApJ*, 710, 1627, doi: [10.1088/0004-637X/710/2/1627](https://doi.org/10.1088/0004-637X/710/2/1627)
- Lépine, S., & Shara, M. M. 2005, *AJ*, 129, 1483, doi: [10.1086/427854](https://doi.org/10.1086/427854)
- Lépine, S., Shara, M. M., & Rich, R. M. 2002, *AJ*, 124, 1190, doi: [10.1086/341783](https://doi.org/10.1086/341783)
- Line, M. R., Teske, J., Burningham, B., Fortney, J. J., & Marley, M. S. 2015, *ApJ*, 807, 183, doi: [10.1088/0004-637X/807/2/183](https://doi.org/10.1088/0004-637X/807/2/183)
- Liu, F., Yong, D., Asplund, M., et al. 2020, *MNRAS*, 495, 3961, doi: [10.1093/mnras/staa1420](https://doi.org/10.1093/mnras/staa1420)
- Liu, M. C., Dupuy, T. J., & Allers, K. N. 2016, *ApJ*, 833, 96, doi: [10.3847/1538-4357/833/1/96](https://doi.org/10.3847/1538-4357/833/1/96)
- Lodders, K. 2002, *ApJ*, 577, 974, doi: [10.1086/342241](https://doi.org/10.1086/342241)
- Lodders, K., & Fegley, B., J. 2006, in *Astrophysics Update 2*, ed. J. W. Mason (Praxis Publishing Ltd), 1, doi: [10.1007/3-540-30313-8_1](https://doi.org/10.1007/3-540-30313-8_1)
- Loutrel, N. P., Luhman, K. L., Lowrance, P. J., & Bochanski, J. J. 2011, *ApJ*, 739, 81, doi: [10.1088/0004-637X/739/2/81](https://doi.org/10.1088/0004-637X/739/2/81)
- Luhman, K. L., Loutrel, N. P., McCurdy, N. S., et al. 2012, *ApJ*, 760, 152, doi: [10.1088/0004-637X/760/2/152](https://doi.org/10.1088/0004-637X/760/2/152)
- Luyten, W. J. 1979, *New Luyten catalogue of stars with proper motions larger than two tenths of an arcsecond; and first supplement; NLTT. (Minneapolis (1979))*; Label 12 = short description; Label 13 = documentation by Warren; Label 14 = catalogue (SAO/NASA)
- Majewski, S. R., Schiavon, R. P., Frinchaboy, P. M., et al. 2017, *AJ*, 154, 94, doi: [10.3847/1538-3881/aa784d](https://doi.org/10.3847/1538-3881/aa784d)
- Mann, A. W., Brewer, J. M., Gaidos, E., Lépine, S., & Hilton, E. J. 2013, *AJ*, 145, 52, doi: [10.1088/0004-6256/145/2/52](https://doi.org/10.1088/0004-6256/145/2/52)
- Mann, A. W., Deacon, N. R., Gaidos, E., et al. 2014, *AJ*, 147, 160, doi: [10.1088/0004-6256/147/6/160](https://doi.org/10.1088/0004-6256/147/6/160)
- Marley, M. S., & Ackerman, A. S. 2001, arXiv e-prints, astro. <https://arxiv.org/abs/astro-ph/0103269>
- Marley, M. S., & Robinson, T. D. 2015, *ARA&A*, 53, 279, doi: [10.1146/annurev-astro-082214-122522](https://doi.org/10.1146/annurev-astro-082214-122522)
- Marley, M. S., Seager, S., Saumon, D., et al. 2002, *ApJ*, 568, 335, doi: [10.1086/338800](https://doi.org/10.1086/338800)
- Marley, M. S., Saumon, D., Visscher, C., et al. 2021, *ApJ*, 920, 85, doi: [10.3847/1538-4357/ac141d](https://doi.org/10.3847/1538-4357/ac141d)
- Marocco, F., Eisenhardt, P. R. M., Fowler, J. W., et al. 2021, *ApJS*, 253, 8, doi: [10.3847/1538-4365/abd805](https://doi.org/10.3847/1538-4365/abd805)
- Minniti, D., Lucas, P., & VVV Team. 2017, *VizieR Online Data Catalog*, II/348
- Morley, C. V., Fortney, J. J., Marley, M. S., et al. 2012, *ApJ*, 756, 172, doi: [10.1088/0004-637X/756/2/172](https://doi.org/10.1088/0004-637X/756/2/172)
- Morley, C. V., Marley, M. S., Fortney, J. J., et al. 2014, *ApJ*, 787, 78, doi: [10.1088/0004-637X/787/1/78](https://doi.org/10.1088/0004-637X/787/1/78)
- Newton, E. R., Charbonneau, D., Irwin, J., et al. 2014, *AJ*, 147, 20, doi: [10.1088/0004-6256/147/1/20](https://doi.org/10.1088/0004-6256/147/1/20)
- Phan-Bao, N., Bessell, M. S., Martín, E. L., et al. 2008, *MNRAS*, 383, 831, doi: [10.1111/j.1365-2966.2007.12564.x](https://doi.org/10.1111/j.1365-2966.2007.12564.x)
- Potter, D., Martín, E. L., Cushing, M. C., et al. 2002, *ApJL*, 567, L133, doi: [10.1086/339999](https://doi.org/10.1086/339999)
- Reid, I. N., Cruz, K. L., Kirkpatrick, J. D., et al. 2008, *AJ*, 136, 1290, doi: [10.1088/0004-6256/136/3/1290](https://doi.org/10.1088/0004-6256/136/3/1290)
- Saumon, D., & Marley, M. S. 2008, *ApJ*, 689, 1327, doi: [10.1086/592734](https://doi.org/10.1086/592734)
- Schmidt, S. J., Cruz, K. L., Bongiorno, B. J., Liebert, J., & Reid, I. N. 2007, *AJ*, 133, 2258, doi: [10.1086/512158](https://doi.org/10.1086/512158)
- Scholz, R. D. 2016, *A&A*, 587, A51, doi: [10.1051/0004-6361/201527965](https://doi.org/10.1051/0004-6361/201527965)

- Skrutskie, M. F., Forrest, W. J., & Shure, M. A. 1987, in *Bulletin of the American Astronomical Society*, Vol. 19, 1128
- Skrutskie, M. F., Cutri, R. M., Stiening, R., et al. 2006, *AJ*, 131, 1163, doi: [10.1086/498708](https://doi.org/10.1086/498708)
- Skrzypek, N., Warren, S. J., Faherty, J. K., et al. 2015, *A&A*, 574, A78, doi: [10.1051/0004-6361/201424570](https://doi.org/10.1051/0004-6361/201424570)
- Smith, L., Lucas, P. W., Burningham, B., et al. 2014, *MNRAS*, 437, 3603, doi: [10.1093/mnras/stt2156](https://doi.org/10.1093/mnras/stt2156)
- Smith, L. C., Lucas, P. W., Contreras Peña, C., et al. 2015, *MNRAS*, 454, 4476, doi: [10.1093/mnras/stv2290](https://doi.org/10.1093/mnras/stv2290)
- Smith, L. C., Lucas, P. W., Kurtev, R., et al. 2018, *MNRAS*, 474, 1826, doi: [10.1093/mnras/stx2789](https://doi.org/10.1093/mnras/stx2789)
- Steinmetz, M., Guiglion, G., McMillan, P. J., et al. 2020, *AJ*, 160, 83, doi: [10.3847/1538-3881/ab9ab8](https://doi.org/10.3847/1538-3881/ab9ab8)
- Stephens, D. C., & Leggett, S. K. 2004, *PASP*, 116, 9, doi: [10.1086/381135](https://doi.org/10.1086/381135)
- Thompson, M. A., Kirkpatrick, J. D., Mace, G. N., et al. 2013, *PASP*, 125, 809, doi: [10.1086/671426](https://doi.org/10.1086/671426)
- Toro, M. E. G., Zhou, Y., & Bowler, B. P. 2022, *Research Notes of the AAS*, 6, 250, doi: [10.3847/2515-5172/aca661](https://doi.org/10.3847/2515-5172/aca661)
- Valenti, J. A., & Piskunov, N. 1996, *A&AS*, 118, 595
- Visscher, C., Lodders, K., & Fegley, Bruce, J. 2006, *ApJ*, 648, 1181, doi: [10.1086/506245](https://doi.org/10.1086/506245)
- Vos, J. M., Allers, K. N., & Biller, B. A. 2017, *ApJ*, 842, 78, doi: [10.3847/1538-4357/aa73cf](https://doi.org/10.3847/1538-4357/aa73cf)
- West, A. A., Hawley, S. L., Bochanski, J. J., et al. 2008, *AJ*, 135, 785, doi: [10.1088/0004-6256/135/3/785](https://doi.org/10.1088/0004-6256/135/3/785)
- West, A. A., Morgan, D. P., Bochanski, J. J., et al. 2011, *AJ*, 141, 97, doi: [10.1088/0004-6256/141/3/97](https://doi.org/10.1088/0004-6256/141/3/97)
- Wilson, J. C., Kirkpatrick, J. D., Gizis, J. E., et al. 2001, *AJ*, 122, 1989, doi: [10.1086/323134](https://doi.org/10.1086/323134)
- Witte, S., Helling, C., & Hauschildt, P. H. 2009, *A&A*, 506, 1367, doi: [10.1051/0004-6361/200811501](https://doi.org/10.1051/0004-6361/200811501)
- Woitke, P., & Helling, C. 2003, *A&A*, 399, 297, doi: [10.1051/0004-6361:20021734](https://doi.org/10.1051/0004-6361:20021734)
- . 2004, *A&A*, 414, 335, doi: [10.1051/0004-6361:20031605](https://doi.org/10.1051/0004-6361:20031605)
- Xuan, J. W., Wang, J., Ruffio, J.-B., et al. 2022, *ApJ*, 937, 54, doi: [10.3847/1538-4357/ac8673](https://doi.org/10.3847/1538-4357/ac8673)
- Zalesky, J. A., Line, M. R., Schneider, A. C., & Patience, J. 2019, *ApJ*, 877, 24, doi: [10.3847/1538-4357/ab16db](https://doi.org/10.3847/1538-4357/ab16db)
- Zhang, Z., Liu, M. C., Marley, M. S., Line, M. R., & Best, W. M. J. 2021a, *ApJ*, 921, 95, doi: [10.3847/1538-4357/ac0af7](https://doi.org/10.3847/1538-4357/ac0af7)
- . 2021b, *ApJ*, 921, 95, doi: [10.3847/1538-4357/ac0af7](https://doi.org/10.3847/1538-4357/ac0af7)
- Zhang, Z. H., Pinfield, D. J., Day-Jones, A. C., et al. 2010, *MNRAS*, 404, 1817, doi: [10.1111/j.1365-2966.2010.16394.x](https://doi.org/10.1111/j.1365-2966.2010.16394.x)